MARTIN MARIETTA ENERGY SYSTEMS LIBRARIES

3 4456 0268420 9

ORNL/TM-10611

ornl

OAK RIDGE
NATIONAL
LABORATORY

MARTIN MARIETTA

Physics Analysis of the TIBER-II Engineering Test Reactor

N. A. Uckan
W. A. Houlberg
S. E. Attenberger
R. A. Dory
D. A. Spong
J. S. Tolliver
J. Sheffield

OAK RIDGE NATIONAL LABORATORY
CENTRAL RESEARCH LIBRARY
CIRCULATION SECTION
4500N ROOM 175
LIBRARY LOAN COPY
DO NOT TRANSFER TO ANOTHER PERSON
If you wish someone else to see this report, send in name with report and the library will arrange a loan.

OPERATED BY
MARTIN MARIETTA ENERGY SYSTEMS, INC.
FOR THE UNITED STATES
DEPARTMENT OF ENERGY

Printed in the United States of America. Available from
National Technical Information Service
U.S. Department of Commerce
5285 Port Royal Road, Springfield, Virginia 22161
NTIS price codes—Printed Copy: A03; Microfiche A01

This report was prepared as an account of work sponsored by an agency of the United States Government. Neither the United States Government nor any agency thereof, nor any of their employees, makes any warranty, express or implied, or assumes any legal liability or responsibility for the accuracy, completeness, or usefulness of any information, apparatus, product, or process disclosed, or represents that its use would not infringe privately owned rights. Reference herein to any specific commercial product, process, or service by trade name, trademark, manufacturer, or otherwise, does not necessarily constitute or imply its endorsement, recommendation, or favoring by the United States Government or any agency thereof. The views and opinions of authors expressed herein do not necessarily state or reflect those of the United States Government or any agency thereof.

ORNL/TM-10611
Dist. Category UC-20

Fusion Energy Division

PHYSICS ANALYSIS OF THE TIBER-II ENGINEERING TEST REACTOR

N. A. Uckan
W. A. Houlberg
S. E. Attenberger
R. A. Dory
D. A. Spong
J. S. Tolliver
J. Sheffield

Presented at the 12th Symposium on Fusion Engineering
Monterey, California, October 12–16, 1987

Data Published: November 1987

Prepared by the
OAK RIDGE NATIONAL LABORATORY
Oak Ridge, Tennessee 37830
operated by
MARTIN MARIETTA ENERGY SYSTEMS, INC.
for the
U.S. DEPARTMENT OF ENERGY
under contract DE-AC05-84OR21400

MARTIN MARIETTA ENERGY SYSTEMS LIBRARIES
3 4456 0268420 9

CONTENTS

ABSTRACT v
1. INTRODUCTION 1
2. CONFINEMENT PROJECTIONS 1
3. BURN DYNAMICS AND VOLT-SECOND CONSUMPTION . . . 6
4. PELLET PENETRATION AND DENSITY PROFILE CONTROL . . 7
5. FAST AND THERMAL ALPHA PARTICLE EFFECTS 11
6. HIGH-ENERGY NEUTRAL BEAM CURRENT DRIVE 15
REFERENCES 17

ABSTRACT

Confinement capability, burn characteristics, heating and fueling requirements, and fast alpha particle effects are assessed for the TIBER-II engineering test reactor (ETR/ITER). Confinement predictions for a wide variety of empirical scaling laws show that ignition in TIBER-II (or similar ETR-like devices) is marginal at 10 MA, whereas the design goal to achieve noninductively driven, steady-state burn with $Q > 5$ can easily be attained. Operation at the higher plasma currents being discussed for ITER or the attainment of higher density limits and/or favorable H-mode scalings improves the ignition capability. Pellet penetration calculations indicate that density profile control with pellets may not be feasible even for pellet velocities up to about 50 km/s; however, density peaking could result from inward pinch effects, as frequently inferred from experiments. The fast alpha contribution to pressure is substantial (10–30%) at TIBER (or any ETR/ITER) burn temperatures (8–20 keV). A relatively low level of fast alpha radial diffusion or a modest level of thermal alpha buildup significantly influences the ignition and steady-state burn capability. The fast alpha population can also modify the background plasma ballooning mode stability boundaries, lowering the beta limit β_{crit}—in particular, operation at the high electron temperatures needed for efficient current drive can exacerbate this effect. The use of high-energy neutral beams offers the promise of two important improvements in projected performance: an effective method for noninductive current drive and a means for controlling the current density profile deep within the plasma, as required for stable operation at high beta levels.

1. INTRODUCTION

The Tokamak Ignition/Burn Experimental Reactor[1] (TIBER-II) is being pursued in the United States (led by Lawrence Livermore National Laboratory) as a candidate for the next-generation Engineering Test Reactor (ETR/ITER). The International Thermonuclear Experimental Reactor (ITER) is the name of the ETR being studied jointly by the United States, the European Community, Japan, and the U.S.S.R. TIBER-II is a compact (3-m major radius), low-cost ETR designed to accommodate noninductive current drive (CD) capability for long-pulse or steady-state ($Q \geq 5$) operation and a double-null poloidal divertor for impurity control and good (H-mode) confinement. Details of the design features are given in Ref. 1. Key design parameters are listed in Table 1.

This paper summarizes the results from physics studies carried out at Oak Ridge National Laboratory (ORNL) in support of the TIBER-II design. The physics models and assumptions used in these studies (see Table 1) are those developed initially for the Compact Ignition Tokamak (CIT)[2–4] by the CIT physics team and the Ignition Physics Study Group (IPSG). The CIT and TIBER-II (ETR/ITER) share the same tokamak data base, although the physics requirements, prime operating conditions, and startup scenario for the CIT differ from those for the noninductively driven TIBER-II, as illustrated in Fig. 1.

Confinement projections are given in Sect. 2. Burn dynamics and volt-second consumption for inductive, pulsed ignition mode are analyzed in Sect. 3. Results from pellet penetration calculations are summarized in Sect. 4. The effects of fast and thermal alpha particles on confinement capability and ballooning mode stability boundaries are given in Sect. 5. Prospects for high-energy neutral beam CD are discussed in Sect. 6.

2. CONFINEMENT PROJECTIONS

The performance of TIBER-II under various confinement scalings has been evaluated using both global analysis[3] and the $1\frac{1}{2}$-D WHIST transport code.[4] Initial cross-checking of the results from these two calculations indicates good agreement on the confinement projections. However, more detailed studies are warranted for examining profile effects—particularly those associated with CD and MHD beta limits. In this section, we present three examples from these calculations: (1) sensitivity of performance to confinement assumptions, (2) ignition capability for a

Table 1. TIBER-II Plasma Parameters and Physics Models[a]

Design Parameters

$R_o = 3.0$ m	$\kappa = 2.22$	$B_o = 6$ T
$a = 0.834$ m	$\delta = 0.4$	$I = 10$ MA

Calculated Parameters

$q_{cyl} \equiv q_* \approx (5a^2 B_o/IR_o)[1 + \kappa^2(1 + 2\delta^2)]/2$	2.5
Density limit (10^{20} m^{-3})	
Murakami, $\langle n_{mu} \rangle \approx 1.5(B/q_* R_o)$	1.2
Greenwald, $\langle n_{GR} \rangle \approx 0.6[\kappa \langle J \rangle]$	2.75
Troyon beta limit ($\beta_{crit} \approx 3I/aB\%$)	6.0

Reference Physics Models and Assumptions

Radial Profiles	$X = X_o\ (1 - r^2/a^2)^{\alpha_X}$; $X = n,\ T$ (and j)
In global model:	$\alpha_n = 0.5$; $\alpha_T = 1.0$; $\alpha_J \approx 3\alpha_T/2 \approx 1.5$
In WHIST code:	$\alpha_n = 0.5$; $\alpha_T =$ transport determined;
	$\alpha_J =$ fixed to maintain $q(0) \geq 1$
Effective Charge	$Z_{eff} = 1.5$ (when specified)
Confinement Scaling	$(1/\tau_E)^2 = (1/\tau_{EOH})^2 + (1/\tau_{Eaux})^2$ with
Neo-Alcator:	$\tau_{EOH} = \tau_{ENA} \approx 0.07\ \langle n_{20} \rangle a R_o^2 q_*$
Kaye-Goldston:	$\tau_{Eaux} = \tau_{EKG}$
	$\approx \dfrac{0.072 f I^{1.24} R_o^{1.65} \kappa^{0.28} \langle n_{20} \rangle^{0.26}}{(P_{heat})^{0.58} a^{0.49} B_o^{0.09}}$
	(L-mode $f = 1$, H-mode $f = 2$;
	average atomic mass $A_i \approx 2.5$)
In global model:	$\tau_{Ee} \approx \tau_{Ei} \approx \tau_E$ (e.g., $\chi_i \approx \chi_{KG+NA}$)
	$\chi_{KG+NA} = [(\chi_{KG})^2 + (\chi_{NA})^2]^{0.5}$
In WHIST code:	$\chi_e \approx \chi_{KG+NA}$; $\chi_i \approx \chi_{iNC} + 0.2\chi_e$
	χ_{KG+NA} = see global model
	χ_{iNC} = ion neoclassical diffusivity
Power degradation:	P_{heat} = (OH + alpha + aux − rad) power
Units	mks, MA, MW, keV, $n_{20} = n_e/10^{20}$ m^{-3}
$\langle n \rangle$	volume-average density
$\langle T \rangle = \langle nT \rangle / \langle n \rangle$	density-weighted average temperature

[a] Design parameters are given in Ref. 1. All others are computed based on the CIT physics assumptions/models given in Refs. 2–4.

ORNL-DWG 87-2402 FED

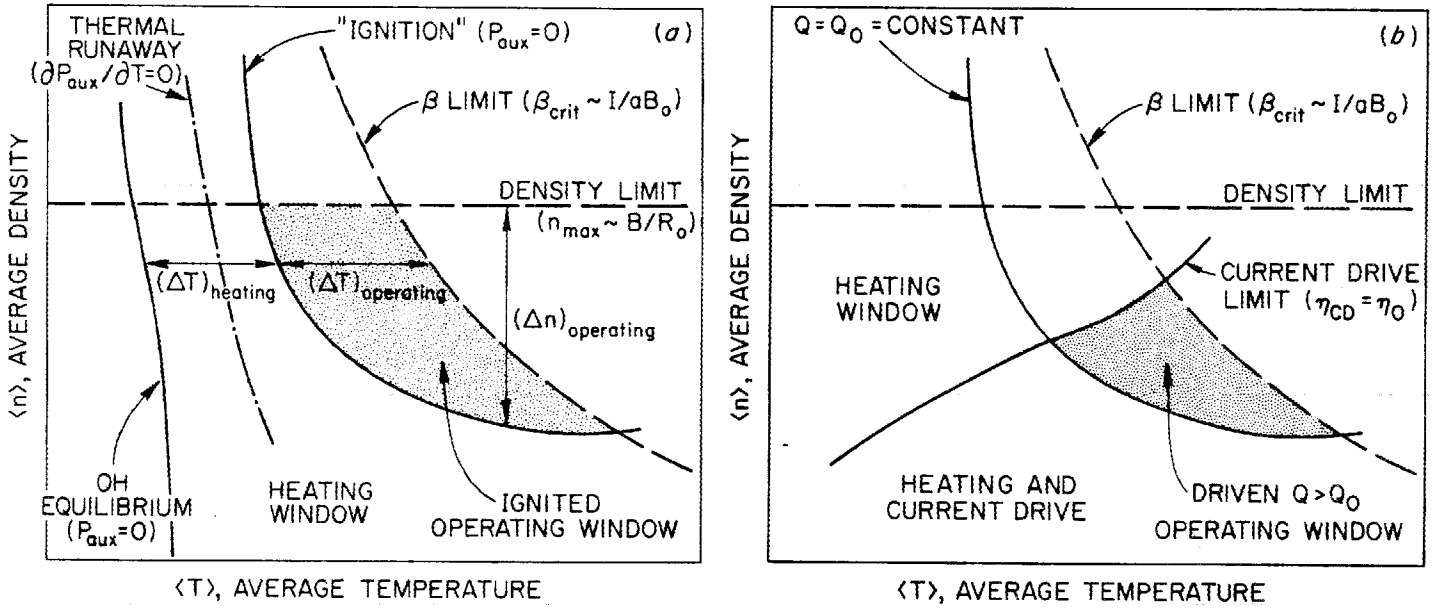

Fig. 1. Typical plasma parameter operating space for (a) inductive (CITs) and (b) noninductive (TIBER-II) current drive.

reference confinement scaling law (see Table 1), and (3) accessibility of the $Q > 5$ regime with noninductive CD.

The difficulty in selecting among common models for confinement scaling is illustrated in Fig. 2, which shows the predictions of a wide variety of empirical transport scalings for TIBER-II (10 MA). The predictions vary widely but, in general, indicate that the TIBER-II design goal of achieving noninductively driven, steady-state burn with $Q \geq 5$ can be attained for most L-mode and nearly all H-mode scalings. The capability to achieve

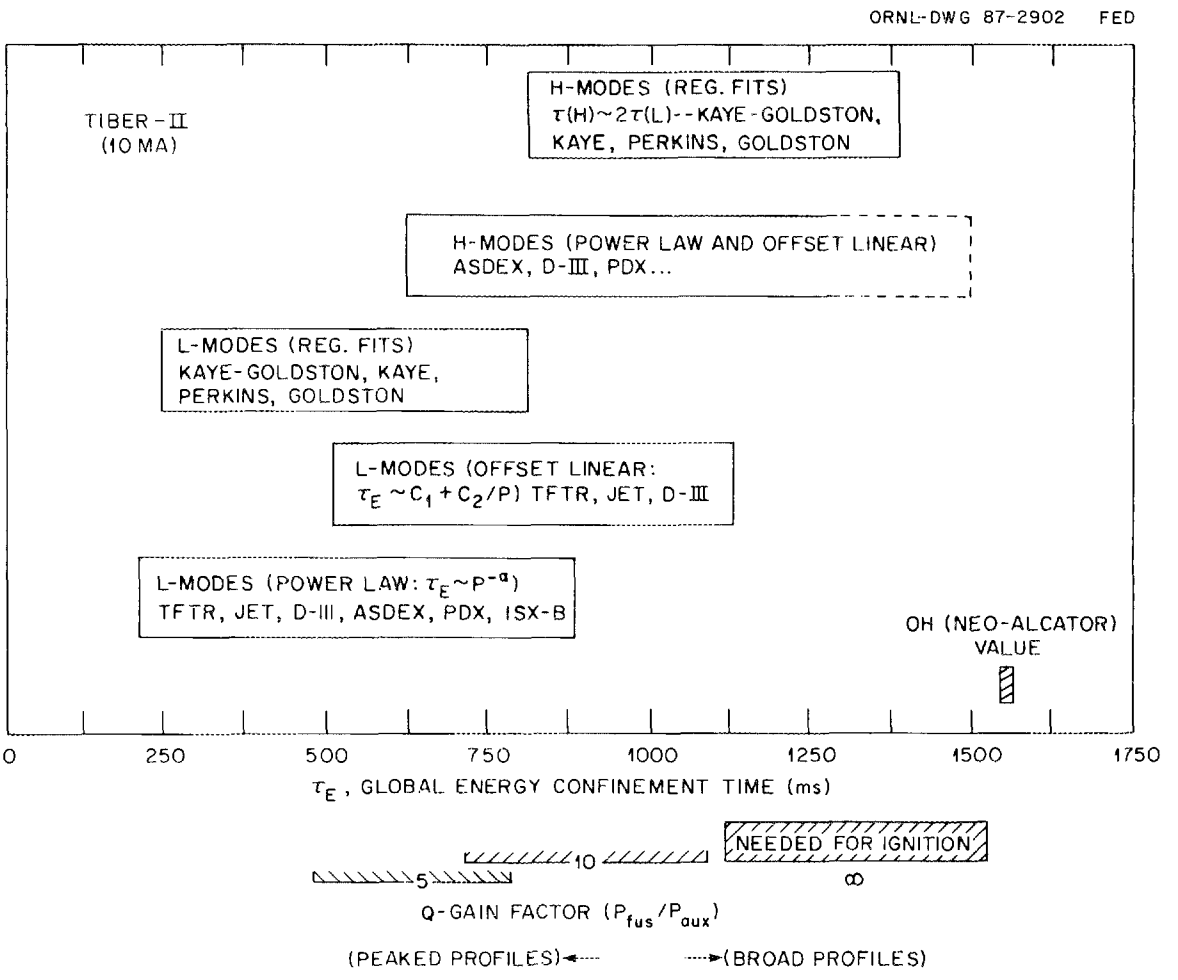

Fig. 2. Confinement projections for a 10-MA TIBER-II for various confinement scaling laws. Reference limits on density ($\langle n \rangle_{\mathrm{mu}}$) and beta (6%) are used to obtain maximum τ_E attainable within the operating window defined in Fig. 1.

ignition may also exist for some H-mode scalings. For a given confinement model, the ignition or high-Q capability can be improved with centrally peaked density or temperature profiles, as illustrated in Fig. 2.

Figure 3 shows ignition contours (in $\langle n \rangle$-$\langle T \rangle$ space) for various L-mode enhancement factors (f) for combined Kaye-Goldston and neo-Alcator scaling ($\chi_e \sim \chi_i \sim \chi_{\mathrm{KG+NA}}$). These contours were obtained from global analysis considering different levels of impurity and thermal alpha concentration. Reference density and beta limits are shown to indicate the extent of the operational boundaries. For densities below the Murakami limit, ignition appears possible only with H-mode-like scalings requiring an L-mode enhancement factor $f \geq 1.8$–2.

Figure 4 shows the steady-state operating contours for 10-MA, noninductive CD operation in TIBER-II. The confinement model is $\chi_e \sim \chi_i \sim \chi_{\mathrm{KG+NA}}$. A reference

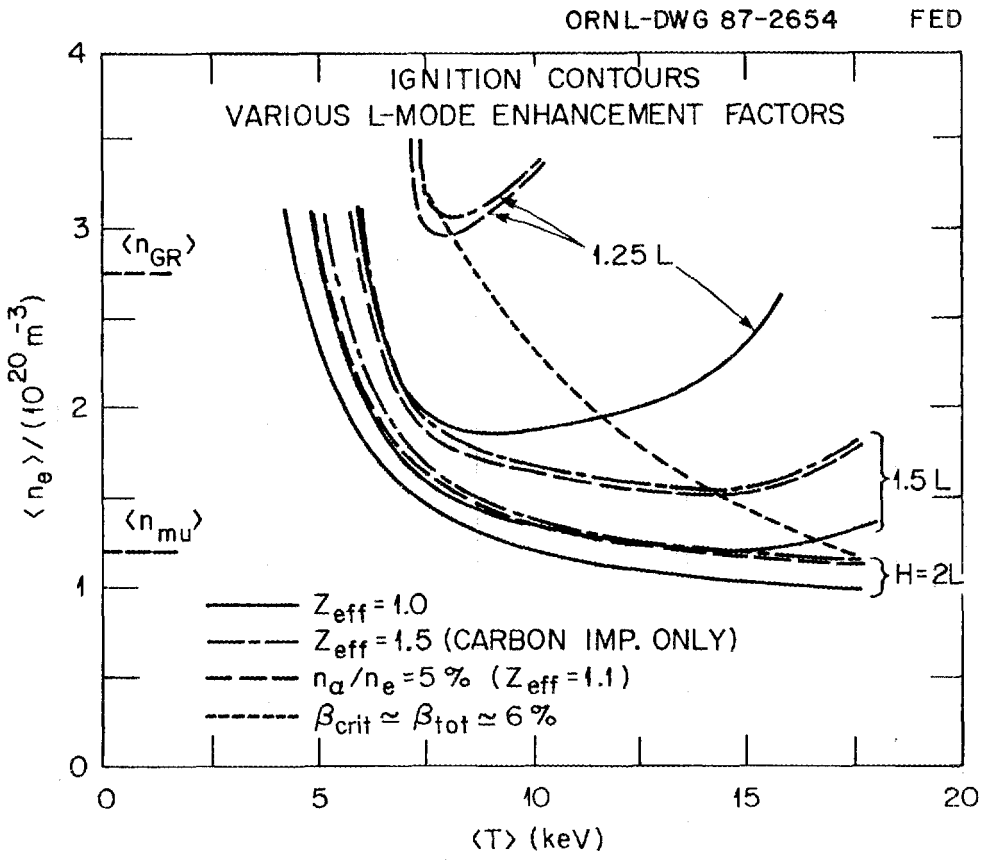

Fig. 3. TIBER-II ignition contours with various L-mode enhancement factors for Kaye-Goldston + neo-Alcator scaling.

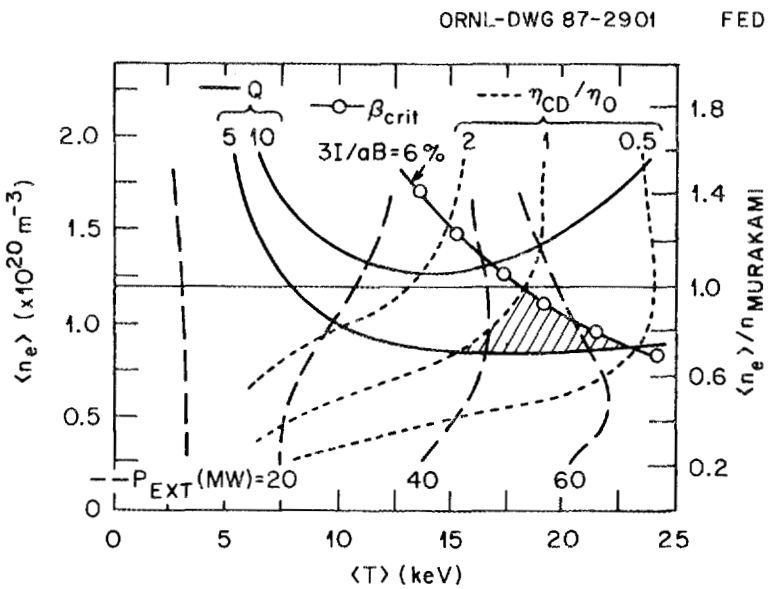

Fig. 4. Steady-state operating contours for a 10-MA noninductive CD mode for various CD efficiencies. The L-mode enhancement factor is ~1.3. Shaded region: $Q > 5$ operating window for a reference CD scheme with $\eta_o = 0.2$ A/W at $\langle n_{mu} \rangle$ and β_{crit}.

CD scheme is taken as a lower hybrid (or neutral beam) type[5,6] with an efficiency $\gamma_{CD} = \gamma_o = n_{20} I R_o / P \sim 0.04 T_e$, yielding $\eta_o = I/P \approx 0.2$ A/W at nominal limits of density ($\langle n_{20} \rangle_{mu} \approx 1.2$) and beta ($\beta_{tot} \approx \beta_{crit} \approx 6\% \Rightarrow \langle T_e \rangle \approx 18$ keV). Shown in Fig. 4 are the contours of (1) $Q = 5$ and 10, (2) external (heating + CD) power required to sustain the plasma (and drive the current) at a given temperature $\langle T \rangle$ and density $\langle n \rangle$, and (3) CD limits for several efficiencies [$\gamma = (0.5\text{–}2)\gamma_o$]. The shaded region in the plot corresponds to a $Q > 5$ operating window for $\gamma \leq \gamma_o$ ($\eta \leq \eta_o$).

3. BURN DYNAMICS AND VOLT-SECOND CONSUMPTION

Using the WHIST transport code, we examine an inductive startup scenario for TIBER-II, scope out the magnetic flux requirements for the poloidal field system, and illuminate other features of the burn dynamics. The reference startup scenario is a 10-s field ramp phase followed by a 4-s auxiliary heating phase. The plasma

evolution is followed for 25 s to observe the thermal excursion and buildup of alpha ash.

The results of a calculation for H-mode confinement are shown in Fig. 5. The toroidal field is ramped from 3 to 6 T while the toroidal current is increased to 10 MA during the field ramp phase, a scenario similar to that employed in CIT.[2] The deuterium fuel is maintained by gas fueling and 90% recycle; the tritium fuel, by injection of 2.2-mm-radius spherical pellets and 90% recycle, as shown in Fig. 5a. Pellet injection is delayed until 2 s before the heating phase to reduce tritium consumption. Only 2–3 pellets are required to bring the tritium density up to the nominal operating density, and a repetition rate of $\approx 1\ \mathrm{s}^{-1}$ is required to sustain the plasma. Although the data shown are for pellets injected at 10 km/s, the results down to $\approx$1.5 km/s are very similar. Accumulation of thermal alphas becomes significant after $\sim$20 s (assumed here to be recycled at 100% for illustrative purposes) with $\langle n_a \rangle / \langle n_e \rangle$ reaching 17% at 25 s.

The heating phase consists of 20 MW of RF power applied 0.2 m outside the magnetic axis with a Gaussian width of 0.4 m. When the auxiliary heating is turned off at 14 s, T_e and T_i continue to rise and the plasma is ignited (Fig. 5b). Thermal runaway is arrested naturally in the vicinity of 20 keV by a combination of the reduced rate of rise in the fusion rate with temperature, the increase in synchrotron radiation losses, burnout of the fuel in the plasma core and replacement by alpha ash, and the reduction in thermal plasma confinement assumed in the Kaye-Goldston H-mode model. Thus $\langle \beta \rangle_{\mathrm{tot}}$ stays below the nominal 6% limit and energetic alphas make up 15% of the total kinetic pressure (see Fig. 5c). There is some flexibility for uncertainties in the confinement model since the baseline fuel density can be adjusted up or down to increase the fusion rate and satisfy the thermal balance (as was done in a series of computational runs that yielded the case presented).

Poloidal flux consumption is dominated by the internal and external components (Fig. 5d); the resistive loss is about 10% of the total 58 V·s required. Dissipative losses from sawtooth activity[7] were found to be negligible for this startup scenario.

4. PELLET PENETRATION AND DENSITY PROFILE CONTROL

Pellet penetration in hot plasmas has long been an issue in the fusion program. The physics goal of penetration to the plasma center (to give maximum external control over the density profile and a possible opportunity to optimize confinement)

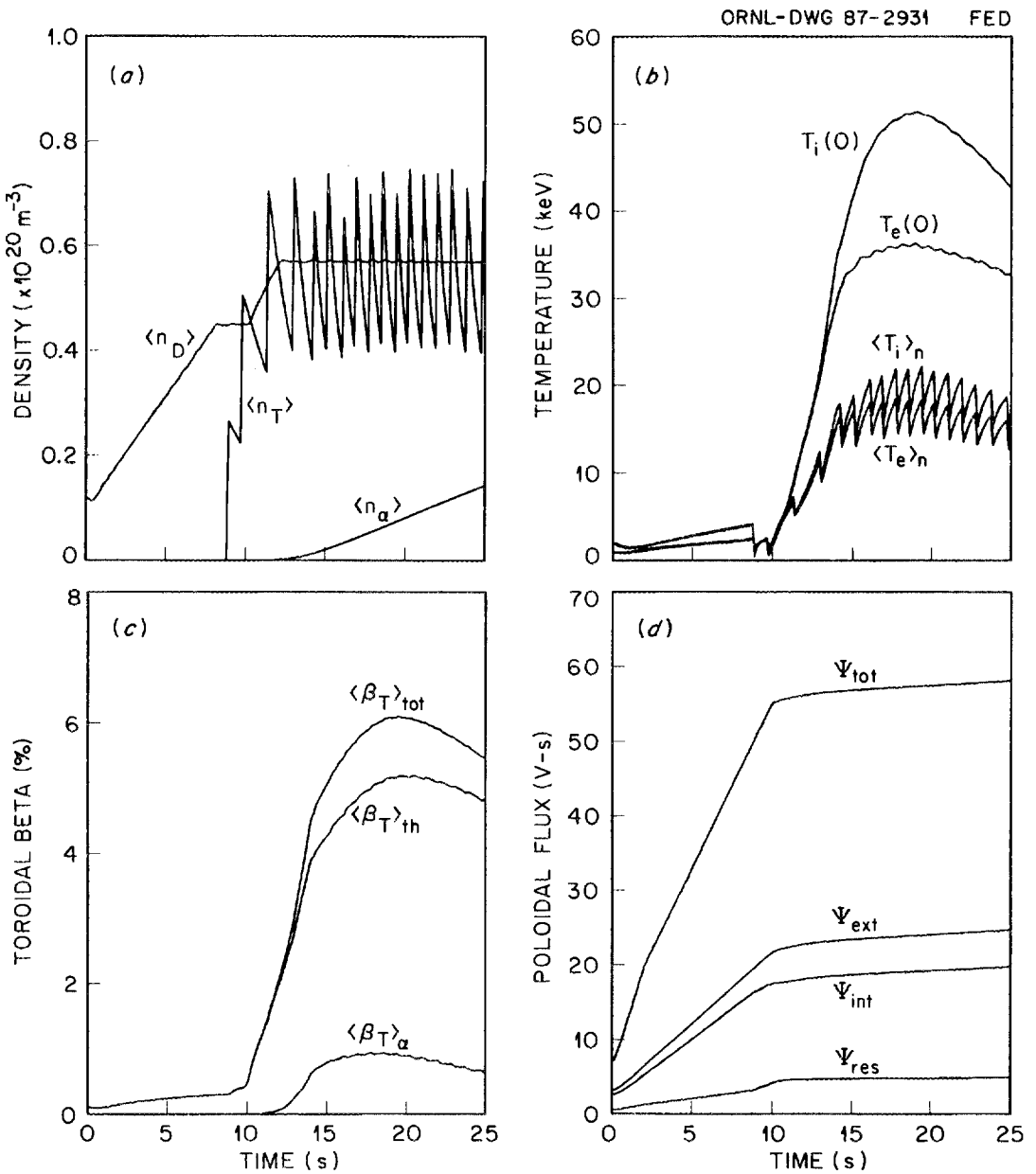

Fig. 5. Dynamics of a 10-MA TIBER-II inductive startup: (a) volume-averaged deuterium, tritium, and thermal alpha densities; (b) central and density-weighted ion and electron temperatures; (c) volume-averaged thermal, fast alpha, and total toroidal beta; and (d) internal, external, resistive, and total poloidal magnetic flux from a Faraday flux balance.

must be weighed against the technology required for producing high-velocity pellets. Both particle and energy confinement have been improved in pellet injection experiments. But the relative roles played by pellet penetration depth and plasma diffusion processes in determining the density profile and plasma confinement properties are not yet well enough understood to allow definitive criteria to be set for pellet penetration and pellet velocity.

Stand-alone pellet penetration studies have been carried out for TIBER-II with an ablation model that has been extensively benchmarked against experimental data from the Joint European Torus (JET).[8] Figure 6 shows the penetration of pellets with a 2-mm effective spherical radius. Each pellet represents about 20% of the Murakami density limit of the TIBER-II plasma. A measure of fueling efficiency is

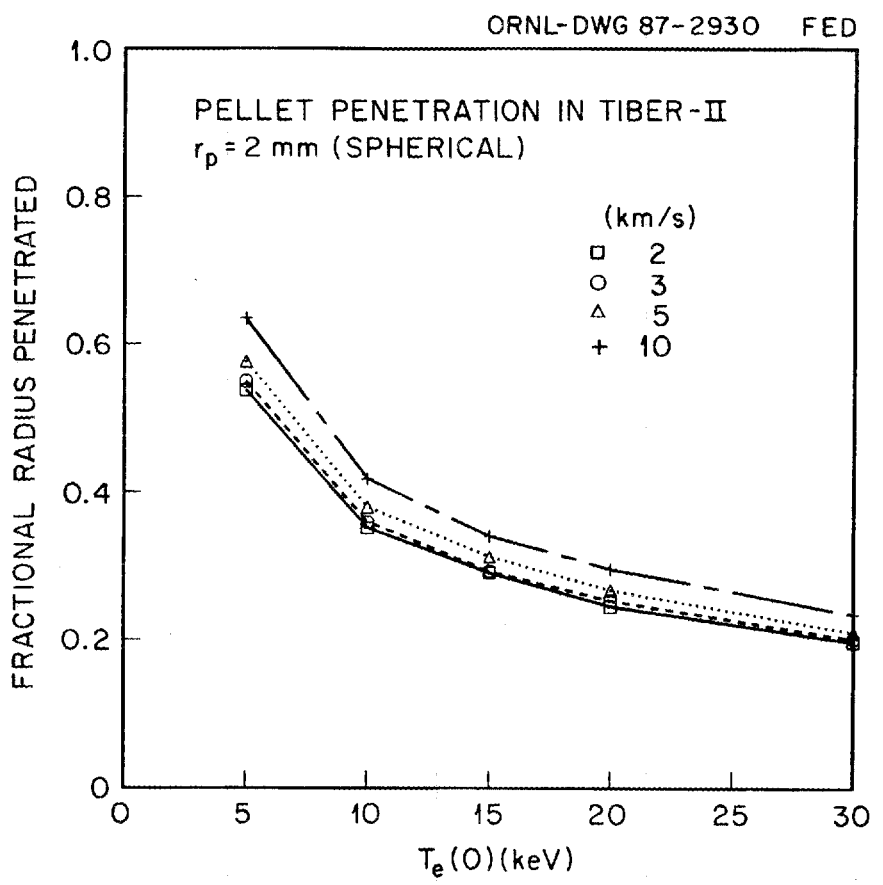

Fig. 6. Fractional radius penetrated by pellets in TIBER-II decreases rapidly with increasing electron temperature and improves weakly with pellet velocity.

the fractional volume penetrated, which is roughly given by $f_V \approx 2f_r(1 - f_r/2)$; i.e., 30% radius penetration gives direct fueling of about 50% of the volume. In Fig. 6, T_e and n_e profiles are assumed parabolic with $n(0) = 1.6 \times 10^{20}$ m^{-3}. Penetration improves only weakly with increasing velocity. Additional shielding effects that may become important in higher-temperature plasmas (e.g., magnetic shielding) could improve the scaling of penetration with pellet velocity. Nonetheless, penetration to or near the magnetic axis would still require extremely high pellet velocities, whose development is problematical, or development of different technologies, such as gun plasma fueling.[9] So it becomes critical to understand (1) the natural tendency of tokamak plasmas to rapidly fill in a hollow density profile after partial pellet penetration and (2) the characteristics of the optimum density profiles.

Figure 7 reflects the influence of the density profile (which is influenced by pellet size and velocity and the particle pinch model) on the ignition curve for TIBER-II

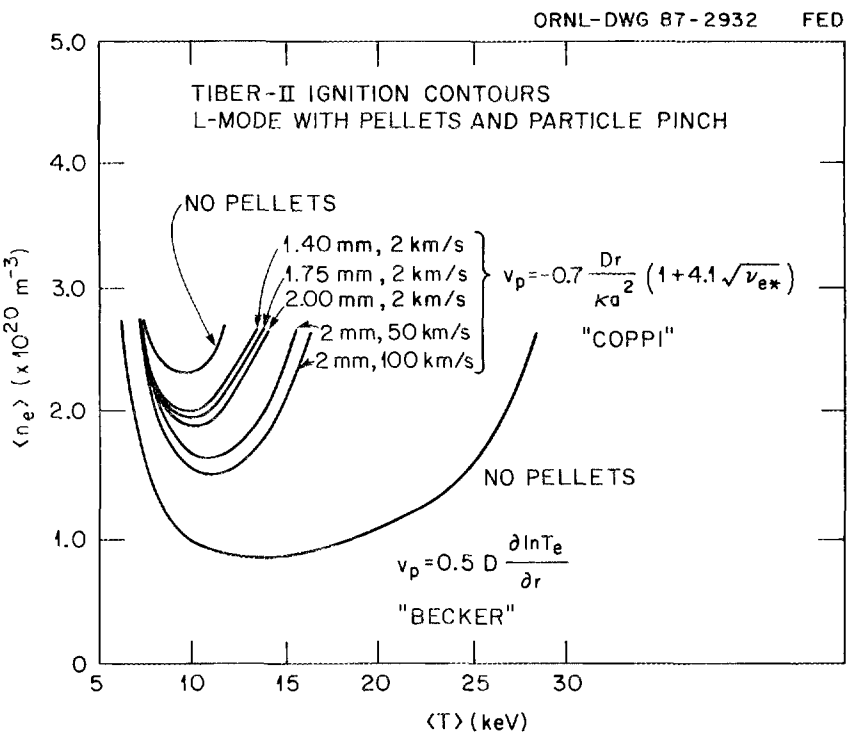

Fig. 7. A more centrally peaked density profile (influenced by pellet size and velocity and inward particle pinch model) improves ignition prospects for these TIBER-II cases with L-mode confinement scaling of the thermal conductivity.

with L-mode confinement. The reference pinch velocity (Coppi model) is given by[10]

$$v_p = -0.7D(r/\kappa a^2)[1 + 4.1(\nu_{e*})^{0.5}] \ ,$$

where D is the particle diffusion coefficient and ν_{e*} is the electron collision frequency normalized to the bounce frequency. This model produces a density profile $n(r) \approx n(0)(1 - r^2/a^2)^{0.5}$ in a plasma fueled by neutral gas injection and recycle. The ignition curve is noticeably lowered for 2-km/s pellets with nominal spherical radii of 1.4, 1.75, and 2 mm. Injection of 5-km/s pellets yields about the same improvement as increasing the pellet size from 1.4 to 2 mm. To get a significant gain in pellet penetration and performance over that for 2 km/s, velocities of 50–100 km/s must be reached. On the other hand, there is a large uncertainty in modeling the pinch term and extrapolating to an ETR-class device, so these conclusions must be viewed with caution. The ignition curve using a pinch model given by Becker[11] for modeling ASDEX data,

$$v_p = 0.5D(\partial \ln T_e/\partial r) \ ,$$

yields a very peaked density profile $[\sim(1 - r^2/a^2)^2]$ even for neutral gas fueling and an ignition curve that more closely resembles H-mode confinement (see Figs. 3 and 7). The density is already so peaked that even 100-km/s pellets do not produce significant additional improvement.

In conclusion, in the absence of a pinch effect, central fueling by pellets would require a pellet velocity that is not credible with present pellet acceleration schemes. However, the effect of pinch terms as now understood makes it credible that pellets with velocities of <10 km/s will fuel adequately, provided (1) the level of pinching persists for larger devices with higher densities and pressures and the addition of burn physics and (2) more sharply peaked density profiles are not required for reasons of CD efficiency or confinement.

5. FAST AND THERMAL ALPHA PARTICLE EFFECTS

The long classical thermalization time for fast alphas in ETR-like plasmas (0.5–1.0 s in the core) gives a significant contribution to the plasma pressure ($\beta_{f\alpha}/\beta_{\rm th} \approx$ 20–30% in the core) and makes the fast alphas vulnerable to radial transport during the thermalization process (especially if $D_\alpha \approx D_{\rm th}$).[12] Figure 8 shows the steady-state fast alpha distribution function $f_\alpha(v, r)$ for a typical TIBER-II plasma with D_α = 0–0.5 m^2/s. Radial diffusion broadens f_α and reduces its magnitude. With

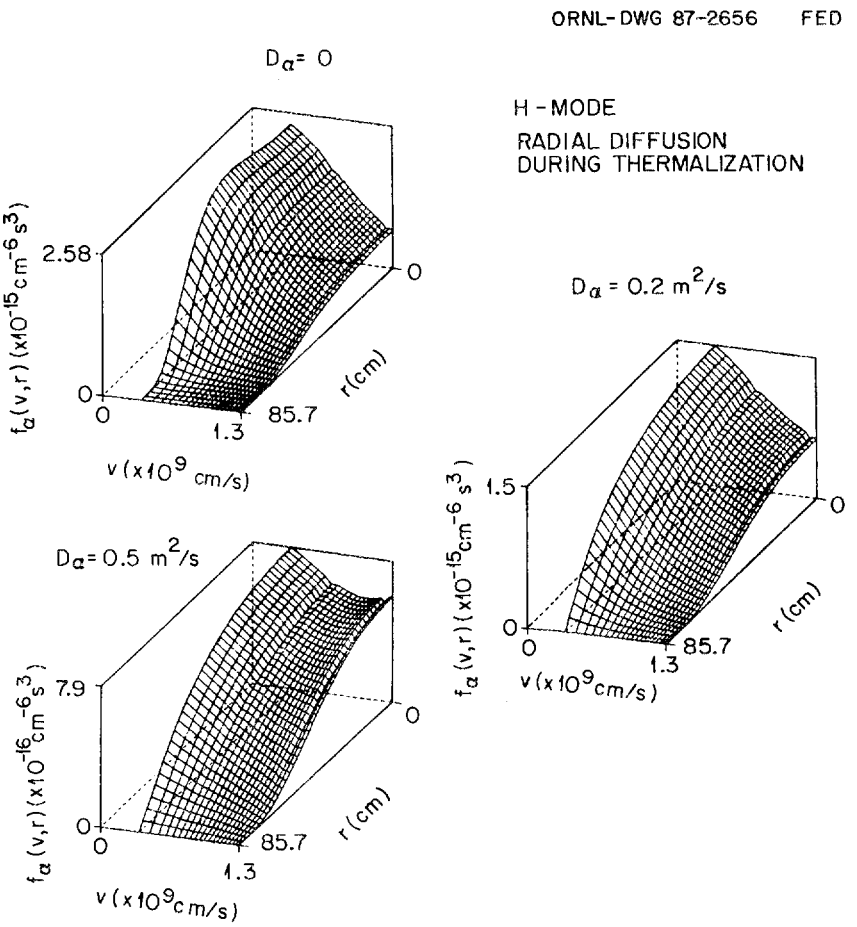

Fig. 8. Steady-state fast alpha distribution function in TIBER-II for H-mode scaling with fast alpha diffusion $D_\alpha = 0$–0.5 m^2/s.

radial fast alpha diffusion at a level comparable to the thermal particle diffusion ($D_\alpha \approx D_{\rm th} \geq 0.5$ m^2/s), it is feasible that an inversion in distribution function ($\partial f_\alpha/\partial v > 0$) could occur, which may drive instabilities.

Figure 9 shows the effect of increasing D_α on the ignited and driven ($Q = 10$) operating regimes of TIBER-II. The results were generated by the WHIST code. An increase in radial diffusion moves the H-mode ignition (or the L-mode $Q = 10$) contours to higher densities, and the operating regime is eliminated if D_α is further increased. For example, for the H-mode case, at densities below the Murakami limit, a small ignition window exists for $D_\alpha = 0$ but is eliminated if $D_\alpha > 0.1$ m^2/s. For higher density limits, however, the ignition window persists but is significantly reduced for $D_\alpha \approx 0.5$ m^2/s.

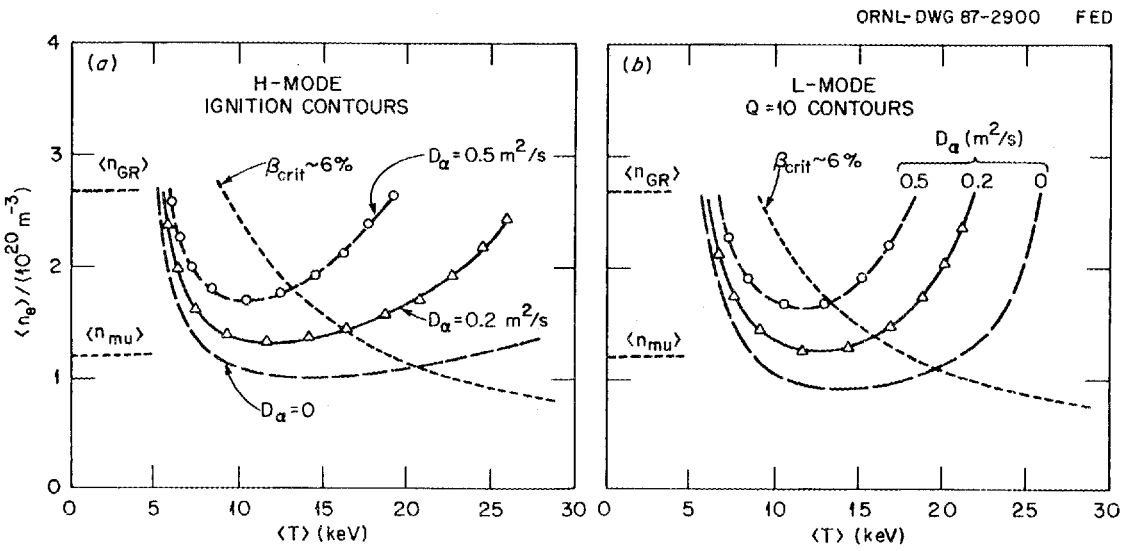

Fig. 9. Influence of fast alpha radial diffusion on (a) H-mode ignition and (b) L-mode $Q = 10$ contours in TIBER-II.

Thermal alpha accumulation dilutes the fuel like any other impurity and reduces fusion power production. In general, for a single impurity of charge Z, the impurity and thermal alpha effects on ignition are nearly the same if $2(n_\alpha/n_e) \approx Z(n_z/n_e) \approx (Z_{\text{eff}} - 1)/(Z - 1)$ (see Fig. 3). Figure 10 shows the influence of thermal alpha concentration ($f_\alpha = n_\alpha/n_e = 0$–$20\%$) on the ignition capability of TIBER-II with an H-mode scaling. Increasing the amount of thermalized alphas (ash) moves the ignition contours to higher densities and eventually eliminates the ignition window within the operational boundaries. For 100% recycling, the time it takes to reach a given level (f_α) of alpha ash is[12]

$$t = (4/n_e\langle\sigma v\rangle_{\text{DT}})f_\alpha/(1 - 2f_\alpha) \ .$$

For a plasma with $n_e = 10^{20}$ m^{-3} and $T \approx 10$ keV, $t \approx 20$ s for 5% and 45 s for 10%. The accumulation time is inversely proportional to nT^2. Thus, at higher n and T, ash buildup is rather fast (see Fig. 5), limiting the burn to a few tens of seconds if no active ash removal scheme is implemented.

The fast alpha population can lead to modifications of the background plasma ballooning mode stability boundaries.[13] One would normally expect the more highly

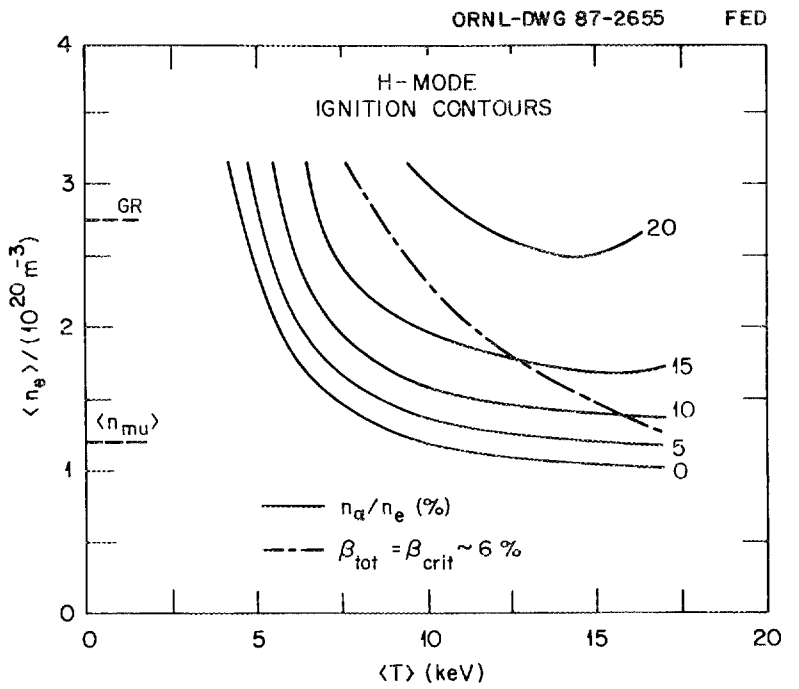

Fig. 10. Influence of thermal alpha concentration (0–20%) on ignition in TIBER-II with H-mode scaling.

peaked fast alpha pressure profiles to destabilize ballooning modes. The kinetic effects from these energetic alphas can be even more important than the profile modifications. One such effect of particular importance is the coupling between the ballooning mode diamagnetic drift and the alpha-banana precessional drift.[13] This is generally destabilizing, since it couples the background plasma more strongly to the bad curvature region on the outside of the tokamak, where the alpha bananas reside. The alphas in the energy range $\langle E_{f\alpha}\rangle/T_i < 150$ (where $\langle E_{f\alpha}\rangle$ is the mean fast alpha energy) are the most destabilizing energy group. Operation at $T_e > 10$–20 keV, as needed for efficient current drive, could exacerbate this effect, lowering $\beta_{\rm crit}$ by as much as a factor of ≥ 2 under certain cases. Calculations indicate that plasma shaping (κ, δ) appears to have much less influence on ballooning mode stability boundaries in the presence of fast alphas than in the ideal case without alphas.

6. HIGH-ENERGY NEUTRAL BEAM CURRENT DRIVE

Current drive using high-energy neutral beams gives promise of two important improvements for projected performance of the TIBER-II (or any ETR/ITER): an effective method for noninductive CD and a means for controlling the current density profile deep within the plasma. The latter is important for stable operation at high plasma energy densities. Preliminary results suggest that neutral beam injection has the flexibility necessary to reproduce current profiles required for stability at the beta levels predicted by the Troyon scaling.

Optimal beam energy for efficient CD[5] is around $E_b/A_bT_e \approx 30$–50. Simple beam penetration analysis shows that, although not optimal, energies around 500 keV may be adequate in small configurations such as TIBER ($R_o \approx 3$ m). For larger tokamaks, obtaining adequate beam penetration would limit operation to low densities ($\sim$ a few $\times\ 10^{19}$ m^{-3}). At low energies, the efficiency of CD is lowered by slowing down on plasma ions below the critical energy ($\sim$330 keV for $T_e \sim$ 20 keV). In the higher energy regime, both the penetration and the efficiency are improved. Estimated CD efficiencies for higher energies are in the range from 0.2 to perhaps 0.3 A/W. These were calculated from (1) simple 0-D slowing-down estimates, (2) work by Cordey[5] and others,[6] and (3) an application of the PROCTR code to provide a full radially resolved treatment. Projected plasma parameters for operating regimes consistent with CD efficiencies in the range 0.1–0.4 A/W are shown in Fig. 4.

An interesting possibility is that of using oppositely directed high- and low-Z beams. This could provide control of the rate of the momentum injection, as well as enhanced CD efficiency. For this purpose and for optimal penetration, the two beams would have about the same energy per amu ($\sim$1 MeV/amu). If oxygen or carbon were used, the required rate of injection would be small, raising the plasma $Z_{\rm eff}$ by $\sim 10^{-3}$ s^{-1} and contributing about 0.5% to the plasma beta ($\beta_b/\beta_{\rm th} \sim 10\%$).

Beam ions with speeds above the plasma Alfvén speed v_a could slow down anomalously rapidly by exciting Alfvén waves.[14] The primary energy source for this unstable coupling of beam free energy lies in regions of positive gradients of the ion velocity distribution: $\partial f_i/\partial v_\parallel$ or $\partial f_i/\partial v_\perp > 0$. The analysis estimated the threshold density above which electron Landau damping can no longer stabilize the coupling.

For "sharp" distributions and *compressional* Alfvén waves, the instability criterion given by Berk et al. is[14] $n_b/n_e > (m_e v_e/m_b v_b)$. For example, consider an ETR or reactor plasma with 10-MA current driven by a 3-MeV neutral deuterium beam in a plasma of density $\sim 10^{20}$ m^{-3}; the threshold density ratio is $\approx 10^{-3}$, so the simple stability criterion might be violated by a factor ~ 2. However, the threshold is modified for the case of a smoother "collisionally equilibrated" energetic ion distribution,

$$n_b/n_e > (m_e v_e/m_b v_b)[(\Delta v_{b\|})^2]/[(v_{b\perp})^4/v_b^4]$$
$$\approx 10^{-3}(0.5^2/0.25^4) \approx 10^{-3} \times (10\text{–}100) \ .$$

Here, we have estimated $\Delta v_{b\|}/v_b \approx 0.5$ and $v_{b\perp}/v_b \approx 0.25$ as typical of a collisional distribution. Since this offers some margin for stability, the simple criterion $v_b > v_a$ is clearly insufficient to rule out energetic neutral beam injection at these high energies.

The requirements for beam destabilization of *shear* Alfvén waves were also estimated:

$$\partial \ln f_b/\partial \ln v_\|^2 > (k_y \rho_b/k_\| r_{\rm nb})(v_\|^2/v_a v_b) \ ,$$
$$n_b/n_e > (m_e/m_i)^{0.5}(m_i v_i/m_b v_b)(\Delta v_b/v_b)^2 (k_\perp \rho_b)^2 (k_\| R_o)^2 \ .$$

Let us assume a collisional distribution, with the left side of the first equation ≈ 0.2 and the ratio of beam distribution radius to plasma radius, $r_{\rm nb}/a$, ≈ 0.04. Suppose the first equation gives the parallel wavelength, while the maximum poloidal wavelength (minimum k_y) is given by $k_y a \approx 1$ and the maximum radial wavelength by $k_\perp a \approx 2.4$. Then the minimum threshold estimate is about the same as the previous one, $n_b/n_e > 10^{-2}$, but is quite sensitive to details. If the stability calculation included desirable improvements to the simple slab model, the threshold might be higher. Better linear analysis with drift orbit corrections and realistic geometry, numerical studies, and experiments are needed to assess the correct stability criteria and determine whether the instability carries a serious potential for reducing beam CD efficiency.

REFERENCES

1. C. D. Henning et al., "TIBER-II Tokamak Ignition/Burn Experimental Reactor—1986 Status Report," UCID-20863, Lawrence Livermore National Laboratory, 1986; also see TIBER-II papers in these proceedings.
2. D. Post et al., "Physics Aspects of the Compact Ignition Tokamak," *Phys. Scr.*, vol. T16, pp. 89–106, 1987; J. Sheffield et al., "Physics Guidelines for Compact Ignition Tokamak," *Fusion Technol.*, vol. 10, pp. 481–490, 1986.
3. N. A. Uckan, "Relative Merits of Size, Field, and Current on Ignited Tokamak Performance," ORNL/TM-10365, Oak Ridge National Laboratory, 1987; N. A. Uckan and J. Sheffield, "A Simple Procedure for Establishing Ignition Conditions in *Tokamak Startup*. New York: Plenum Press, 1986, pp. 45–72.
4. W. A. Houlberg, "Plasma Engineering Assessment of Compact Ignition Experiments," in *Proceedings of the 11th Symposium on Fusion Engineering,* 1985, pp. 50–55; W. A. Houlberg et al., "Contour Analysis of Fusion Reactor Performance," *Nucl. Fusion*, vol. 22, pp. 935–945, 1982.
5. See J. G. Cordey, "A Review of Non-Inductive Current Drive Theory," *Plasma Phys.*, vol. 26, pp. 123–132, 1983.
6. See N. J. Fisch, "Theory of Current Drive in Plasmas," *Rev. Mod. Phys.*, vol. 59, pp. 175–234, 1987.
7. W. A. Houlberg, "Volt-Second Consumption in Tokamaks with Sawtooth Activity," *Nucl. Fusion*, vol. 27, pp. 1009–1020, 1981.
8. W. A. Houlberg et al., "Neutral and Plasma Shielding Model for Pellet Ablation," ORNL/TM-10556, Oak Ridge National Laboratory, 1987.
9. See papers on "Plasma Guns and Cluster Beams," in *Proceedings of the Fusion Fueling Workshop,* CONF-771129, pp. 1–21, 1977; A. W. Leonard et al., "Trapping of Gun-Injected Plasma by a Tokamak," *Phys. Fluids*, vol. 30, pp. 2877–2884, 1987; L. J. Perkins et al., "Deep Penetration Fueling of Reactor-Grade Plasmas with Accelerated Compact Toroids," UCRL-96894, Lawrence Livermore National Laboratory, 1987.
10. B. Coppi and N. Sharky, "Model for Particle Transport in High-Density Plasmas," *Nucl. Fusion*, vol. 21, pp. 1363–1382, 1981.
11. G. Becker, "Anomalous Inward Particle Flux in Tokamaks Due to a Thermoelectric-Type Effect," *Nucl. Fusion*, vol. 27, pp. 11–17, 1987.

12. N. A. Uckan et al., "Influence of Fast Alpha Diffusion and Thermal Alpha Buildup on Tokamak Reactor Performance," ORNL/TM-10612, Oak Ridge National Laboratory, 1987.
13. D. A. Spong et al., "Effects of Alpha Particle Population on Tokamak Ballooning Stability," *Phys. Scr.*, vol. T16, pp. 18–26, 1987.
14. H. L. Berk et al., "Microinstability Theory of Two-Energy-Component Toroidal Systems," *Nucl. Fusion*, vol. 15, pp. 819–843, 1975.

ORNL/TM-10611
Dist. Category UC-20

INTERNAL DISTRIBUTION

1–5. S. E. Attenberger
6. L. A. Berry
7. B. A. Carreras
8–12. R. A. Dory
13. J. L. Dunlap
14. J. D. Galambos
15–19. W. A. Houlberg
20. H. C. Howe
21. J. F. Lyon
22. M. Murakami
23. S. L. Painter
24. Y-K. M. Peng
25. R. L. Reid
26. M. J. Saltmarsh
27. T. E. Shannon
28–32. J. Sheffield
33–37. D. A. Spong
38–42. J. S. Tolliver
43–52. N. A. Uckan
53. T. Uckan
54–55. Laboratory Records Department
56. Laboratory Records, ORNL-RC
57. Document Reference Section
58. Central Research Library
59. Fusion Energy Division Library
60–61. Fusion Energy Division Publications Office
62. ORNL Patent Office

EXTERNAL DISTRIBUTION

63. Office of the Assistant Manager for Energy Research and Development, U.S. Department of Energy, Oak Ridge Operations Office, P. O. Box E, Oak Ridge, TN 37831
64. J. D. Callen, Department of Nuclear Engineering, University of Wisconsin, Madison, WI 53706-1687
65. J. F. Clarke, Director, Office of Fusion Energy, Office of Energy Research, ER-50 Germantown, U.S. Department of Energy, Washington, DC 20545
66. R. W. Conn, Department of Chemical, Nuclear, and Thermal Engineering, University of California, Los Angeles, CA 90024
67. S. O. Dean, Fusion Power Associates, Inc., 2 Professional Drive, Suite 249, Gaithersburg, MD 20760
68. H. K. Forsen, Bechtel Group, Inc., Research Engineering, P. O. Box 3965, San Francisco, CA 94105
69. J. R. Gilleland, L-644, Lawrence Livermore National Laboratory, P.O. Box 5511, Livermore, CA 94550
70. R. W. Gould, Department of Applied Physics, California Institute of Technology, Pasadena, CA 91125

71. R. A. Gross, Plasma Research Laboratory, Columbia University, New York, NY 10027
72. D. M. Meade, Princeton Plasma Physics Laboratory, P.O. Box 451, Princeton, NJ 08544
73. M. Roberts, International Programs, Office of Fusion Energy, Office of Energy Research, ER-52 Germantown, U.S. Department of Energy, Washington, DC 20545
74. W. M. Stacey, School of Nuclear Engineering and Health Physics, Georgia Institute of Technology, Atlanta, GA 30332
75. D. Steiner, Nuclear Engineering Department, NES Building, Tibbetts Avenue, Rensselaer Polytechnic Institute, Troy, NY 12181
76. R. Varma, Physical Research Laboratory, Navrangpura, Ahmedabad 380009, India
77. Bibliothek, Max-Planck Institut für Plasmaphysik, Boltzmannstrasse 2, D-8046 Garching, Federal Republic of Germany
78. Bibliothek, Institut für Plasmaphysik, KFA Jülich GmbH, Postfach 1913, D-5170 Jülich, Federal Republic of Germany
79. Bibliothek, KfK Karlsruhe GmbH, Postfach 3640, D-7500 Karlsruhe 1, Federal Republic of Germany
80. Bibliotheque, Centre de Récherches en Physique des Plasmas, Ecole Polytechnique Federale de Lausanne, 21 Avenue des Bains, CH-1007 Lausanne, Switzerland
81. F. Prévot, CEN/Cadarache, Departement de Récherches sur la Fusion Contrôlée, F-13108 Saint-Paul-lez-Durance Cedex, France
82. Bibliothèque, CEN/Cadarache, F-13108 Saint-Paul-lez-Durance Cedex, France
83. Documentation S.I.G.N., Departement de la Physique du Plasma et de la Fusion Contrôlée, Association EURATOM-CEA, Centre d'Etudes Nucléaires, B.P. 85, Centre du Tri, F-38041 Grenoble, France
84. Library, Culham Laboratory, UKAEA, Abingdon, Oxfordshire, OX14 3DB, England
85. Library, JET Joint Undertaking, Abingdon, Oxfordshire OX14 3EA, England
86. Library, FOM-Instituut voor Plasmafysica, Rijnhuizen, Edisonbaan 14, 3439 MN Nieuwegein, The Netherlands
87. Library, Institute of Plasma Physics, Nagoya University, Chikusa-ku, Nagoya 464, Japan
88. Library, International Centre for Theoretical Physics, P.O. Box 586, I-34100 Trieste, Italy
89. Library, Centro Richerche Energia Frascati, C.P. 65, I-00044 Frascati (Roma), Italy
90. Library, Plasma Physics Laboratory, Kyoto University, Gokasho, Uji, Kyoto, Japan

91. Plasma Research Laboratory, Australian National University, P.O. Box 4, Canberra, A.C.T. 2601, Australia
92. Library, Japan Atomic Energy Research Institute, Tokai Research Establishment, Tokai, Naka-gun, Ibaraki-ken 311-02, Japan
93. Library, Japan Atomic Energy Research Institute, Naka Research Establishment, Naka-machi, Naka-gun, Ibaraki-ken, Japan
94. G. A. Eliseev, I. V. Kurchatov Institute of Atomic Energy, P. O. Box 3402, 123182 Moscow, U.S.S.R.
95. V. A. Glukhikh, Scientific-Research Institute of Electro-Physical Apparatus, 188631 Leningrad, U.S.S.R.
96. I. Shpigel, Institute of General Physics, U.S.S.R. Academy of Sciences, Ulitsa Vavilova 38, Moscow, U.S.S.R.
97. D. D. Ryutov, Institute of Nuclear Physics, Siberian Branch of the Academy of Sciences of the U.S.S.R., Sovetskaya St. 5, 630090 Novosibirsk, U.S.S.R.
98. V. T. Tolok, Kharkov Physical-Technical Institute, Academical St. 1, 310108 Kharkov, U.S.S.R.
99. Library, Academia Sinica, P.O. Box 3908, Beijing, China (PRC)
100. R. A. Blanken, Experimental Plasma Research Branch, Division of Applied Plasma Physics, Office of Fusion Energy, Office of Energy Research, ER-542, Germantown, U.S. Department of Energy, Washington, DC 20545
101. K. Bol, Princeton Plasma Physics Laboratory, P.O. Box 451, Princeton, NJ 08544
102. R. A. E. Bolton, IREQ Hydro-Quebec Research Institute, 1800 Montee Ste.-Julie, Varennes, P.Q. JOL 2P0, Canada
103. D. H. Crandall, Experimental Plasma Research Branch, Division of Applied Plasma Physics, Office of Fusion Energy, Office of Energy Research, ER-542, Germantown, U.S. Department of Energy, Washington, DC 20545
104. R. L. Freeman, GA Technologies, Inc., P.O. Box 85608, San Diego, CA 92138
105. K. W. Gentle, RLM 11.222, Institute for Fusion Studies, University of Texas, Austin, TX 78712
106. R. J. Goldston, Princeton Plasma Physics Laboratory, P.O. Box 451, Princeton, NJ 08544
107. J. C. Hosea, Princeton Plasma Physics Laboratory, P.O. Box 451, Princeton, NJ 08544
108. S. W. Luke, Division of Confinement Systems, Office of Fusion Energy, Office of Energy Research, ER-55, Germantown, U.S. Department of Energy, Washington, DC 20545

109. E. Oktay, Division of Confinement Systems, Office of Fusion Energy, Office of Energy Research, ER-55, Germantown, U.S. Department of Energy, Washington, DC 20545
110. D. Overskei, GA Technologies, Inc., P.O. Box 85608, San Diego, CA 92138
111. R. R. Parker, Plasma Fusion Center, NW 16-288, Massachusetts Institute of Technology, Cambridge, MA 02139
112. W. L. Sadowski, Fusion Theory and Computer Services Branch, Division of Applied Plasma Physics, Office of Fusion Energy, Office of Energy Research, ER-541, Germantown, U.S. Department of Energy, Washington, DC 20545
113. J. W. Willis, Division of Confinement Systems, Office of Fusion Energy, Office of Energy Research, ER-55, Germantown, U.S. Department of Energy, Washington, DC 20545
114. A. P. Navarro, Division de Fusion, CIEMAT, Avenida Complutense 22, E-28040 Madrid, Spain
115. Laboratory for Plasma and Fusion Studies, Department of Nuclear Engineering, Seoul National University, Shinrim-dong, Gwanak-ku, Seoul 151, Korea
116. M. A. Abdou, School of Engineering and Applied Science, 6288 Boelter Hall, University of California, Los Angeles, CA 90024
117. C. C. Baker, Argonne National Laboratory, 9700 South Cass Avenue, Argonne, IL 60439
118. C. Bolton, Office of Fusion Energy, Office of Energy Research, ER-55 Germantown, U.S. Department of Energy, Washington, DC 20545
119. D. R. Cohn, Plasma Fusion Center, NW 16-140, Massachusetts Institute of Technology, Cambridge, MA 02139
120. B. Coppi, 77 Massachusetts Avenue, Massachusetts Institute of Technology, Cambridge, MA 02139
121. R. C. Davidson, 77 Massachusetts Avenue, Massachusetts Institute of Technology, Cambridge, MA 02139
122. N. A. Davies, Office of Fusion Energy, Office of Energy Research, ER-55 Germantown, U.S. Department of Energy, Washington, DC 20545
123. S. A. Eckstrand, Office of Fusion Energy, Office of Energy Research, ER-55 Germantown, U.S. Department of Energy, Washington, DC 20545
124. A. J. Favale, MS-A0126, *Grumman Corporation*, P.O. Box 31, Bethpage, NY 11714
125. T. K. Fowler, L-640, Lawrence Livermore National Laboratory, P.O. Box 5511, Livermore, California 94550
126. H. P. Furth, Princeton Plasma Physics Laboratory, P.O. Box 451, Princeton, NJ 08544
127. C. D. *Henning*, L-640, Lawrence Livermore National Laboratory, P.O. Box 5511, Livermore, California 94550

128. T. R. James, Office of Fusion Energy, Office of Energy Research, ER-55 Germantown, U.S. Department of Energy, Washington, DC 20545
129. R. A. Krakowski, CTR-12, Mail Stop 641, Los Alamos National Laboratory, P.O. Box 1663, Los Alamos, NM 87545
130. G. L. Kulcinski, Room 439, Department of Nuclear Engineering, Engineering Research Building, University of Wisconsin, 1500 Johnson Drive, Madison, WI 53706
131. B. G. Logan, L-644, Lawrence Livermore National Laboratory, P.O. Box 5511, Livermore, California 94550
132. J. A. Maniscalo, R1/2128, TRW Defense and Space Systems, One Space Park, Redondo Beach, CA 90278
133. G. H. Miley, Nuclear Engineering Department, University of Illinois, Urbana, IL 61801
134. D. B. Montgomery, Plasma Fusion Center, NW 16-140, Massachusetts Institute of Technology, Cambridge, MA 02139
135. D. E. Post, Princeton Plasma Physics Laboratory, P.O. Box 451, Princeton, NJ 08544
136. P. H. Rebut, JET Joint Undertaking, Abingdon, Oxon OX14 3EA, England
137. F. L. Ribe, College of Engineering, FL-10, AERL Bldg., University of Washington, Seattle, WA 98195
138. D. Ross, Fusion Research Center, The University of Texas, Austin, TX 78712
139. P. H. Rutherford, Princeton Plasma Physics Laboratory, P.O. Box 451, Princeton, NJ 08544
140. J. A. Schmidt, Princeton Plasma Physics Laboratory, P.O. Box 451, Princeton, NJ 08544
141. R. D. Stambaugh, GA Technologies, Inc., P.O. Box 85608, San Diego, CA 92138
142. P. M. Stone, Office of Fusion Energy, Office of Energy Research, ER-55 Germantown, U.S. Department of Energy, Washington, DC 20545
143. H. Weitzner, Courant Institute of Mathematical Sciences, New York University, 251 Mercer Street, New York, NY 10012

144–220. Given distribution as shown in TIC-4500, Magnetic Fusion Energy (Distribution Category UC-20)